Disorder and localization dynamics in polymorphs of the molecular semiconductor pentacene probed by *in situ* micro-Raman spectroscopy and molecular dynamics simulations

Masahiko Ando,[1,*] Makoto Yoneya,[2] Thomas B. Kehoe,[3] Hiroyuki Ishii,[4] Takashi Minakata,[5] Masahiro Kawasaki,[1] Claudia M. Duffy,[3] Richard Phillips,[3] and Henning Sirringhaus[3]

[1]*R&D group, Hitachi, Ltd., 1–280 Higashi-Koigakubo, Kokubunji, Tokyo 185–8601, Japan*
[2]*Advanced Industrial Science and Technology, 1-1-1 Umezono, Tsukuba, 305–8568, Japan*
[3]*Cavendish Laboratory, JJ Thomson Avenue, Cambridge, CB3 0HE, United Kingdom*
[4]*University of Tsukuba, 1-1-1 Tennodai, Tsukuba, Ibaraki 305–8573, Japan*
[5]*Asahi-Kasei Corporation, R&D Centre, 2-1 Samejima, Fuji, Shizuoka, 416–0934, Japan*

(Received 8 October 2017; revised manuscript received 8 January 2019; published 19 February 2019)

To reveal the relationship between microstructural disorder and charge localization dynamics in a van-der-Waals-bonded molecular semiconductor, the electrical properties of field-effect transistors with zone-cast pentacene films were characterized by using *in situ* micro-Raman spectroscopy to monitor the films' intermolecular and intramolecular vibrations. Transformations from a high-temperature phase with reduced molecular vibration along the long axis that were induced by electron localization in pentacene molecules at the channel interface and transformations from a low-temperature phase with increased molecular vibration that were induced by the electron delocalization were clearly observed under gate-bias stress, photoexcitation, and thermal annealing. Multilayer molecular dynamics simulations revealed that electrons should be localized in each pentacene molecule to stabilize the low-temperature phase and that the intramolecular Raman peak corresponds to the amount of out-of-plane molecular displacement that is most influential to charge localization and mobility reduction induced by fluctuating transfer integrals. We propose a unified picture to describe the relationship between out-of-plane structural disorder and charge localization dynamics in pentacene polymorphs.

DOI: 10.1103/PhysRevMaterials.3.025601

I. INTRODUCTION

Solution-processable small-molecule semiconductors with carrier mobilities well exceeding 1 cm^2/Vs have been developed [1]. Once the major extrinsic factors limiting the mobility of crystalline molecular semiconductors are eliminated (factors such as chemical impurities and defects in the crystal and its interfaces with electrodes and gate dielectric), mobility is no longer limited by such static disorder but rather by the dynamic disorder of the transfer integrals induced by thermal fluctuations of semiconductor molecules weakly packed by van der Waals force [2,3]. Here, Fratini *et al.* proposed a transient localization scenario in which a charge becomes localized in space as the carrier wave function evolves in response to the rearrangement of the surrounding molecular fragments and vibrations in the associated intermolecular electronic coupling [4]. Localization and subsequent release of the localized charge occur on the timescale of the slow, thermally activated molecular motions. Fratini *et al.* further proposed a map plotting the transient localization length of different molecular crystals and showed how their mobilities can be identified by considering only the sign and relative magnitude of the electronic coupling between neighboring molecules [5]. This map clearly visualizes why the hole mobility in pentacene, a benchmark molecular semiconductor, is surprisingly low and cannot be easily explained by conventional theories. Experimentally, Eggeman *et al.* used a transmission electron microscopy technique, thermal diffuse scattering in electron diffraction patterns, to directly observe thermal molecular motion in several classes of high-mobility crystalline organic semiconductors such as 6,13-bistriisopropyl-silylethynyl pentacene (TIPS-pentacene) [6]. They revealed that the dominant thermal motion in TIPS-pentacene corresponds to a translational vibration of the pentacene fragment in the direction of the long axis and that this vibration makes the mobility of TIPS-pentacene lower than those of other small molecules wherein the amplitudes of their intermolecular vibrations are reduced because of the side chains attached to the axis of the molecule's highest-amplitude vibration [7]. The above theoretical and experimental approaches were reviewed in a study of the low-frequency vibrations and their role in charge transport in high-mobility organic semiconductors including pentacene [8].

Our purpose in the present study is to investigate the effect of such dynamic and static disorder on the electronic properties of pentacene polymorphs (differently assembled forms of the same molecules) [9,10]. We recently proposed an intrinsic charge trapping (permanent localization) mechanism in pentacene due to the static polymorphic disorder, one that is based on results we obtained by investigating the structure-property relationship in zone-cast pentacene (ZCPEN) field-effect transistor (FET) under gate-bias stress by using *in situ* micro-Raman spectroscopy in the low-frequency region in combination with a theoretical simulation [11]. Our molecular

*Author to whom correspondence should be addressed: masahiko.ando.ph@hitachi.com

dynamics (MD) simulation revealed that the dominant thermal motion in pentacene corresponds to a translational vibration in the direction of the long axis and it is suppressed by the charge localization. The dynamic disorder of the charge-trapping molecules becomes frozen (becomes static) at room temperature. Our findings suggested that the permanent localization is due to self-trapping with the static disorder induced by Coulomb repulsive force between electrons localized in neighboring pentacene molecules with mutual transfer integrals reduced by the disorder itself.

In the present study, to probe the dynamic disorder as well as the static disorder of different polymorphs, we used *in situ* micro-Raman spectroscopy to monitor the intramolecular vibration modes in the high-frequency region together with the intermolecular vibration modes in the low-frequency region *In situ* micro-Raman spectroscopy is a powerful technique for investigating the microstructures of a van-der-Waals-bonded molecular system because it is fast and nondestructive [12–18]. It has been suggested that a comparison of the Raman peaks in these two different frequency regions would give useful indications on the intra- and interlayer order or in-plane and out-of-plane molecular motion in molecular semiconductor systems [17,18]. In the case of pentacene, the Raman peaks in the low-frequency region (10–50 cm^{-1}) are attributed to the intermolecular lattice phonon modes, while the Raman peaks in the high-frequency region (1140–1190 cm^{-1}) are attributed to the intramolecular C-H bending modes at the ends of pentacene molecules. Brillante's and Girlando's groups collaboratively revealed a strong correlation between the intra- and intermolecular vibration peaks of different pentacene polymorphs by comparing thin-film and single-crystal samples [17,18]. They reported that the intramolecular vibration peaks differ among pentacene polymorphs and can be used to identify polymorphs: 1154, 1156, and 1158 cm^{-1} for thin-film (TF), high-temperature (HT), and low-temperature (LT) phases, respectively (right panel of Fig. 3 in Ref. [17]). They stressed that a comparison of the low-frequency and high-frequency regions of the Raman spectra gives useful information on the intra- and interlayer order of the TF phase. Furthermore, we found that the 1163−cm^{-1} peak, which is weak in the LT phase, is enhanced by charge trapping. Our MD simulation revealed that the long-axis molecular displacement becomes larger in the phase order TF, HT, LT, and charged LT, and the intramolecular peak correlates well with the vertical molecular displacement and the interaction strength between molecules in adjacent layers. We observed an irreversible transformation from the LT phase to the HT phase accompanying increased mobility after bias-stress and thermal annealing, which is reasonable since the mobility increased with decreasing the vertical molecular displacement as confirmed both theoretically [5] and experimentally [7].

On the basis of an examination of field-effect mobilities, transfer integral disorder, and the intra-Raman peak as a function of the MD-simulated vertical molecular displacement in the LT and HT phases together with those reported for the TF phase, we propose a unified picture for the structure-property relationship in pentacene polymorphs that arises from the conflict between in-plane and out-of-plane dynamic disorders induced by competition between van der Waals force, thermal vibration, and electronic Coulomb repulsive force. This picture treats the transient and permanent localizations on the same footing by taking account of the out-of-plane dynamic and static disorder, and it clarifies how the transient localization due to dynamical molecular motions originates from *Anderson localization* [19]. Our previously proposed charge trapping (permanent localization) mechanism of static disorder [11] is seamlessly situated in this picture.

II. EXPERIMENT

The structure and fabrication process of the pentacene films and devices were the same as in Ref. [11]. Details of the solution process of pentacene films are described elsewhere [20,21]. Prior to performing the bias-stressing routine, the devices were annealed at 130 °C in nitrogen for 1 h to stabilize their performance. Field-effect mobilities up to 0.7 cm^2/Vs were achieved after annealing. After bias stressing the devices, which degrades their performance, the same annealing conditions were used to restore their performance to the original level. We used a pristine device before annealing in order to observe the mobility increase that accompanied the irreversible phase transition occurring during annealing after the bias stress.

The herringbone stacking of the pentacene molecules in the LT phase is different from that of the HT phase [see Fig. 1(c) of Ref. [11] and Fig. 14]. The monolayers of the two structures are the same, but the molecules in adjacent layers are aligned in the LTform, whereas they are offset in the HTform (see the dashed ovals in Fig. 14). Siegrist *et al.* discuss these forms in detail in Ref. [22]. The HT form has a vibrational mode at 44 cm^{-1}, whereas the corresponding mode in the LT form is shifted to 50 cm^{-1} [16]. As described later, the Raman spectra clearly shows that a transformation between the two structures emerges under bias stress. It has recently been revealed that the dynamic correlation between molecules in adjacent layers is lost in the TF phase [17]. Therefore, the aligned feature of the LT phase is unique among the three polymorphs and should be the origin of the structural disorder along the long axis (Δl_c) in the LT phase, which is almost one order of magnitude larger than in the HT phase as revealed by our MD simulation [23].

In situ electrical and Raman measurements were made in a microchamber (Linkam LTSE350) filled with a nitrogen atmosphere. A HeNe 632.8-nm laser with a power less than 500 μW was focused to a spot approximately 1 μm in diameter at the sample, and Raman signals in the Stokes shift region from 10 to 1700 cm^{-1} were measured with a Horiba Jobin Yvon T64000 spectrometer. An X-Y stage was used to scan the sample to build up a Raman map of selected areas. White light with wavelengths between 450 and 1000 nm (from a xenon lamp filtered by indium-oxide-coated glass) was used to illuminate the samples without causing UV degradation or IR heating. Relatively high gate bias-stress voltages, $V_{st} = \pm 40$ V ($\approx$1 MV/cm), were applied for a maximum of 15 h with drain and source voltages kept at −5 and 0 V, respectively. Details of the HF (intramolecular) Raman spectra were acquired using a WITec Raman microscope (100x objective) and a 632.8-nm excitation from a HeNe laser [24]. Samples were measured in air, and low laser power (less than 500 μW) was used in order to avoid damaging the samples.

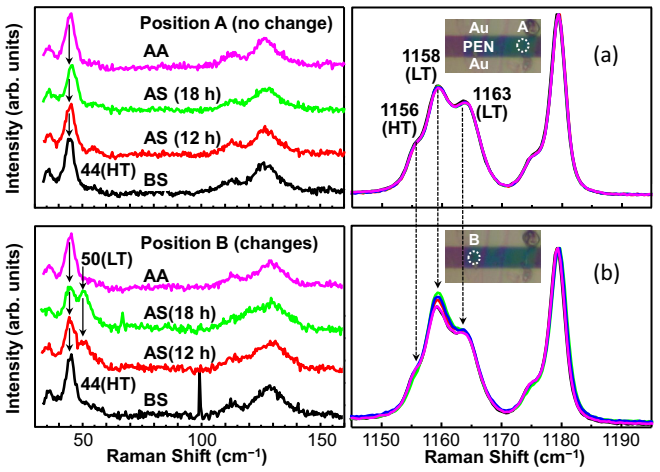

FIG. 1. Intermolecular (low-frequency) and intramolecular (high-frequency) vibration Raman peaks from different areas (A, B) of the same ZCPEN film before and after bias stress (BS, AS) and after thermal annealing (AA).

The spectra were averaged over 25 accumulations (5 sec per accumulation).

We conducted multilayer MD simulations of a flexible all-atom model of pentacene to investigate the effect of trapped charge on the stability of polymorphs in pentacene. The simulations were performed for a temperature of 293 K and pressure of 1 atm; the details are given in the Supplemental Material [25] and elsewhere [23,26]. In contrast to the usual MD unit cell for pentacene, which has two-layer stacks with a 3×2 monolayer totaling 12 molecules, periodic boundary conditions, and a fixed volume and shape, we used a relatively large unit cell composed of 12 stacks of 12×7 monolayers that was 17-nm thick and had 1008 pentacene molecules in order to take account of the fluctuations along the long-axis direction in which we were mostly interested. Furthermore, the MD cell had a fully variable shape to allow for structural fluctuations and transitions between the polymorphs.

The transfer integrals, J, were calculated using Eq. (10) in Ref. [27]. The calculated values were mostly comparable to those reported in Ref. [5] (Table S1 in the Supplemental information) and quantitatively reproduced the experimentally obtained field-effect mobility of pentacene and the temperature-dependent change in nature from band-like to thermally activated as a function of the magnitude of external static disorder [28,29].

III. RESULTS AND DISCUSSION

A. Effect of bias stress on Raman peak correlation

As shown in Fig. 1, there was a clear correlation between the intermolecular peaks and the intramolecular peaks. The figure compares the intermolecular (low-frequency) and intramolecular (high-frequency) vibration Raman peaks in two different areas (A and B in the insets showing the optical images of the device) of the same ZCPEN film before bias stress (BS), after BS (AS), and after thermal annealing (AA). Peaks corresponding to the HT and LT phases are observed in both areas, at 44, 50, 1156, 1158, and 1163 cm^{-1}. There is no

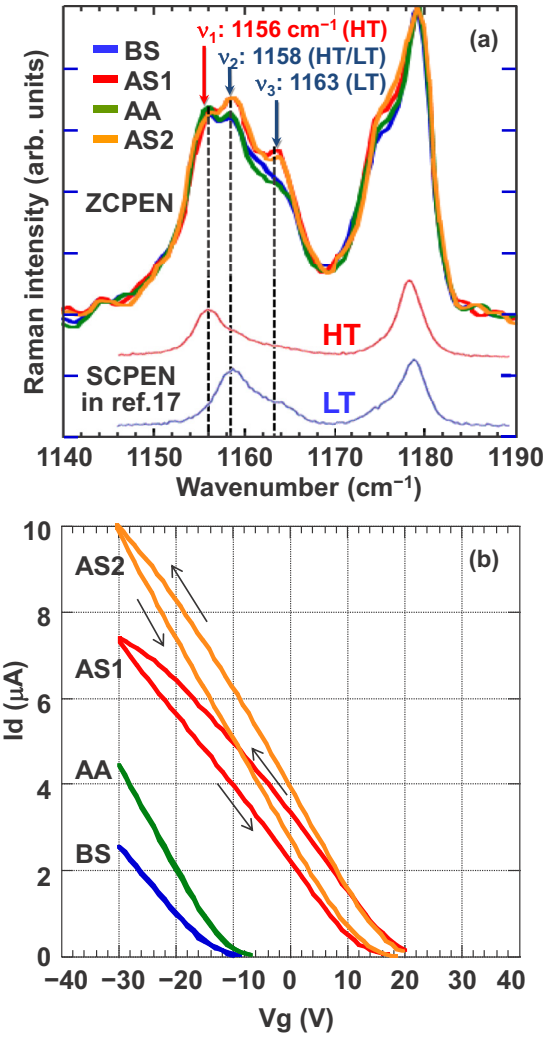

FIG. 2. (a) Comparison of intramolecular vibration Raman peaks of ZCPEN films and SCPEN, the latter taken from Fig. 3 of Ref. [17]. Reversible change of peaks at 1154 cm^{-1} (ν_1), 1158 cm^{-1} (ν_2), and 1163 cm^{-1} (ν_3) before stress (BS), after first stress (AS1), after annealing (AA), and after second stress (AS2); (b) corresponding change in transfer characteristics.

1154 cm^{-1} peak corresponding to the TF phase, which means that the ZCPEN films must have been composed of a mixture of HT and LT phases. The inter- and intramolecular peaks both change in area A; those at 50, 1158, and 1163 cm^{-1} for the LT phase increase after the BS and decrease after thermal annealing, whereas they do not change in area B. These results indicate that the changes in the intramolecular peaks in the HT region are due to those of polymorphs, as clarified by the corresponding changes in the intermolecular peaks. Such a correlation between inter- and intramolecular peaks has been reported only in single-crystal pentacene (SCPEN) samples [17,18], and this indicates the high crystallinity of the zone-cast films [20].

Figure 2(a) compares the intramolecular peaks of ZCPEN films under BS and thermal annealing with those of SCPEN reported in Fig. 3 of Ref. [17] and Fig. 6 of Ref. [18]. Three peaks at 1156, 1158, and 1163 cm^{-1} are clearly seen

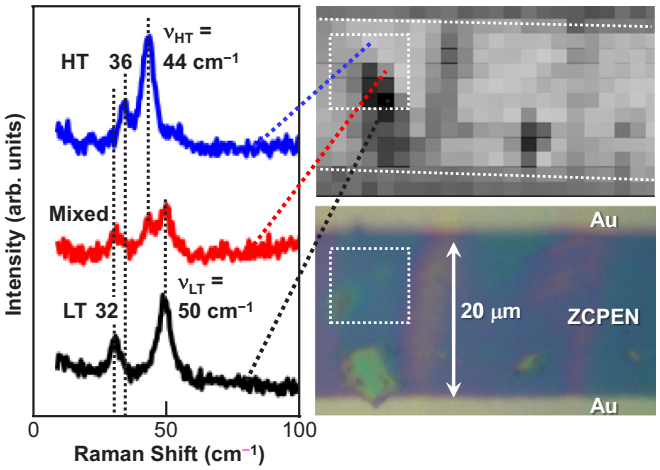

FIG. 3. Raman mapping and corresponding optical planar image of the sample (right). Typical intermolecular Raman peaks for HT, LT, and mixed phases, including the 44 and 50 cm^{-1} peaks used to make the mapping (left). 36 and 32 cm^{-1} subpeaks for the HT and LT phases are also shown.

in the intramolecular Raman spectra of both films; the 1156 cm^{-1} peak corresponds to the HT phase and the 1158 and 1163 cm^{-1} peaks mainly correspond to the LT phase. In the following, we will refer to these intramolecular vibration peaks as ν_1, ν_2, and ν_3, respectively.

The transfer (Id-Vg) characteristics before and after the first bias stress (BS, AS1), after thermal annealing (AA: 120 °C, 1 h), and after the second BS (AS2) are shown in Fig. 2(b). The slope of the transfer characteristics increases after annealing, since a pristine FET sample with ZCPEN and without a thermal treatment after deposition was used for this measurement. The mobilities calculated from the slopes of the transfer curves before stress (BS) and after annealing (AA) are 0.48 and 0.7 cm^2/Vs, respectively. The increase in mobility is irreversible, since the slope of the transfer curve after the second BS (AS2) is as high as that after annealing (AA). Threshold voltage shifts after consecutive BSs indicate charge trapping at the interface between the ZCPEN and the gate insulator. ν_2 and ν_3, which are dominant in the LT phase, increase with charge trapping after BS (AS) and decrease with charge detrapping after thermal annealing (AA). These peaks can be assigned to the C-H in-plane vibration of atoms located at the ends of the molecules [13]. These results indicate that the charge trapping induced by BS not only caused a microstructural transformation from the HT phase to the LT phase; it also strengthened the interaction between molecules in adjacent layers.

Low-frequency Raman spectra and a Raman map of the ZCPEN film of the FET device before stress are shown in the top left and right panels of Fig. 3; the corresponding optical plan view is shown in the panel at the bottom right. The bottom spectrum, labeled "LT", has peaks at 32 and 50 cm^{-1}, which correspond to those seen in Raman spectra from PEN single crystals in the LT phase, which is the most stable phase deep inside the crystals at room temperature [30]. The top spectrum, labeled "HT", has two different peaks, at 36 and 44 cm^{-1}, which are typical of the HT phase usually observed at the surface of single crystals formed at high temperature [30]. A Raman map, made by assigning a brightness gradient to the ratio of the intensity of the dominant peak at $\nu_{HT} = 44$ cm^{-1} for the HT phase divided by that of the peak at $\nu_{LT} = 50$ cm^{-1} for the LT phase, of the area shown in the corresponding optical image (right-bottom) indicates that ZCPEN films are composed of HT-phase PEN (bright regions) with LT-phase PEN (dark regions) dispersed in the HT-phase matrix. This finding is reasonable since 100-nm-thick films with a free surface should correspond to the surface regions of crystals (see Fig. 4 of Ref. [30]); an MD simulation has shown that that the LT phase is unstable and tends to transform into the HT phase in PEN thin films because of the interaction between molecules in the two surface monolayers, one adjacent to air and the other adjacent to dielectric substrate [23]. The intermediate region between the two phases shows a "mixed phase" in which all the peaks in both phases are superimposed in the Raman spectra, as is observed in single crystals [30]. It should be noted that the gradual change from the HT phase to the LT phase over a distance of 5 to 10 μm, with 1-μm resolution and a 2-μm step, indicates that this mixed phase is not an artefact of the spatial resolution of the Raman measurement but rather a real mixture of HT and LT phases.

Figure 4 shows magnified Raman maps corresponding to the white-dotted square area (5 μm^2 square) in the right panel of Fig. 3 before stress, after stress, and after annealing from left to right (top), the relative Raman peak intensities, ν_{LT}/ν_{HT}, along the vertical dotted lines in the Raman maps (middle), and cross-sectional images of the polymorph distribution in pentacene films (bottom). These results clearly indicate that the relative amount of LT phase, which increased AS, decreased AA to well below the original value before stress (BS). This reduction was irreversible and it accompanied the mobility increase shown in the increase of slope of the Id-Vg curve from BS to AA in Fig. 2(b). Although we only observed a charge-induced transformation in the transitional regions between the two polymorphs, we expect that it should occur uniformly at the pentacene/dielectric interface, as shown schematically at the bottom of Fig. 4, since Kelvin probe measurements have shown that the charges are uniformly trapped at the interface [31].

B. Photoexcitation effect on correlation of Raman peaks

To elucidate the microscopic structure dynamics during the phase transformation in pentacene polymorphs, the correlation between the intermolecular (low-frequency) and intramolecular (high-frequency) Raman peaks was further investigated by monitoring the transient properties induced by photoexcitation. The transient characteristics of the Id-Vg curves after removing the BS in the dark and subsequent photoexcitation are shown in Fig. 5(a), and the corresponding relative threshold voltage shift (ΔVth) and trapped charge $\Delta Q(=C \times \Delta Vth)$ are shown in Fig. 5(b). Here, the threshold voltage at time t, $Vth(t)$, is defined as the Vth obtained by extrapolating the linear part of the transfer curve at time t to the horizontal voltage axis, while $\Delta Vth(t)$ is defined as $Vth(t) - Vth(0)$ just after the BS, as shown in Fig. 5(a). C is the dielectric capacitance of the gate insulator. The

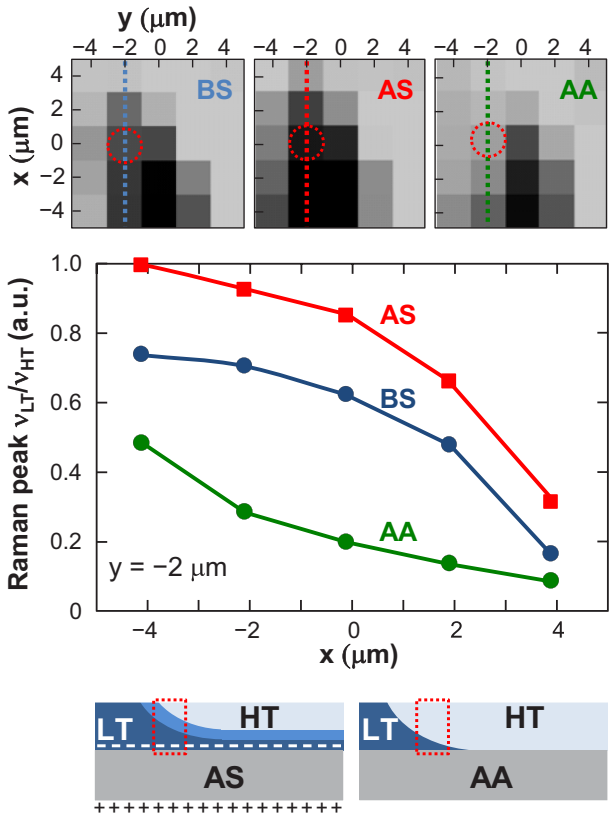

FIG. 4. Magnified Raman maps corresponding to the white dotted square area (5 μm^2 square) in the right panel of Fig. 3 before stress, after stress, and after annealing from left to right (top), relative Raman peak intensities, ν_{LT}/ν_{HT}, along the vertical dotted lines shown in the Raman maps (middle), and sectional images of polymorph distribution in pentacene films (bottom). After stress (AS), the LT phase (dark blue) penetrates the HT phase (light blue) on the right with accumulated electrons (–) at the gate insulator interface; the moderately light blue area is the extended LT phase. After annealing (AA), all of the LT phase that had extended to the channel interface transforms back into the HT phase after photoexcitation releases all of the trapped electrons. The red dotted rectangles correspond to the cross section of the red dotted circular areas shown in the Raman mappings at the top.

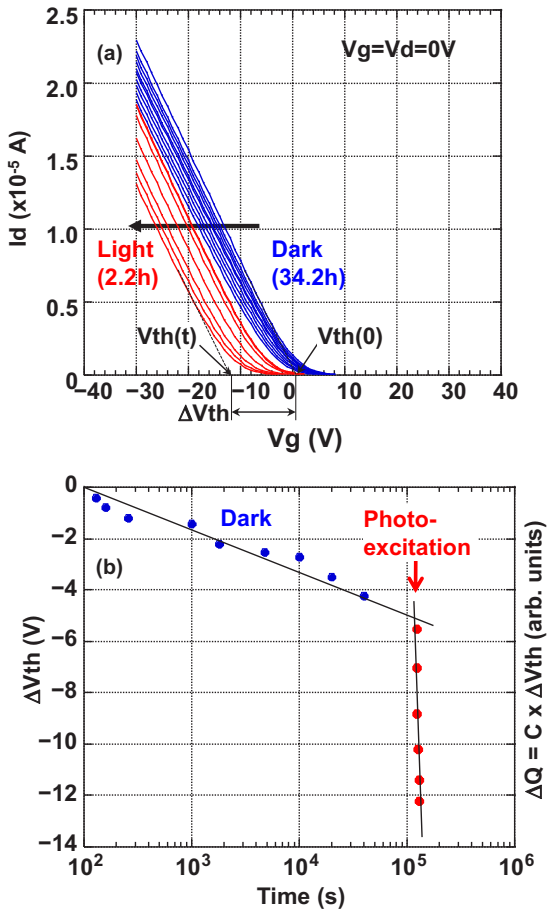

FIG. 5. (a) Temporal recovery of Id-Vg curves shifted by trapped charge after removing BS in the dark and subsequent photoexcitation; (b) change in trapped charge, ΔQ, in the dark and subsequent photoexcitation.

sharp change in slope just after the photoexcitation indicates that the photoexcitation drastically accelerated the otherwise relatively gradual decay of ΔQ in the dark.

The corresponding transition in the intermolecular vibrational peaks in the low-frequency region around 25–75 cm^{-1} and the relative Raman peak intensities, ν_{LT}/ν_{HT}, after removing the BS in the dark (0–4200 s) and subsequent photoexcitation (4800–7500 s) are shown in Fig. 6. As our previous results indicate (Fig. 2 of Ref. [11]), even after switching off the BS, the HT phase continued to transform into the LT phase because the height of the 50 cm^{-1} peak continued to increase. Since there was no external field, this observation confirms that the transformation is not due to the external electric field and it must be connected in some way to the presence of electrons at the interface. We speculate that some of the released electrons might have diffused into the bulk and enhanced the phase transformation by becoming trapped.

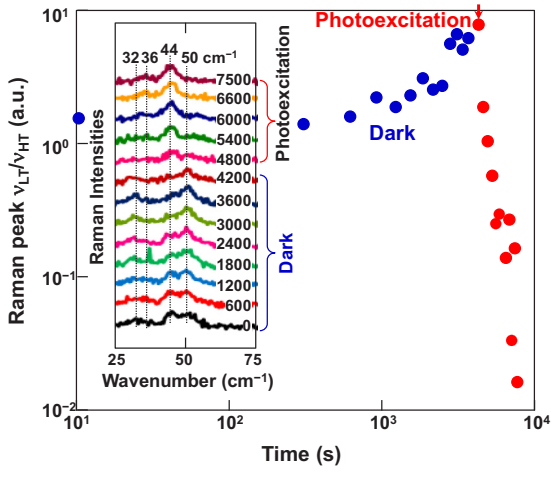

FIG. 6. Relative intermolecular Raman peak intensity (ν_{LT}/ν_{HT}) as a function of time in the dark and in photoexcitation. The inset shows time evolution of intermolecular Raman peaks in the low-frequency region after applying a gate BS for 18 h at a gate voltage $Vg = +40$ V, drain voltage $Vd = -5$ V. The gate BS was turned off at $t = 0$ s. Photoexcitation was started at $t = 4300$ s to release electrons trapped in pentacene.

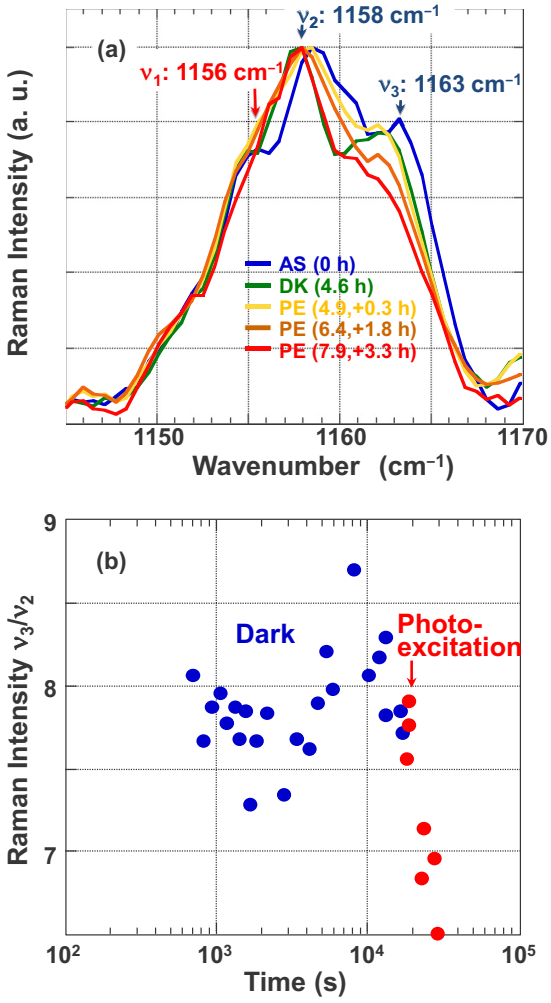

FIG. 7. (a) Intramolecular Raman peaks at 1154 (ν_1), 1158 (ν_2), and 1163 cm^{-1} (ν_3) after removing BS in the dark and subsequent photoexcitation; (b) Relative intramolecular Raman peak intensity (ν_3/ν_2) as a function of time in the dark and in photoexcitation.

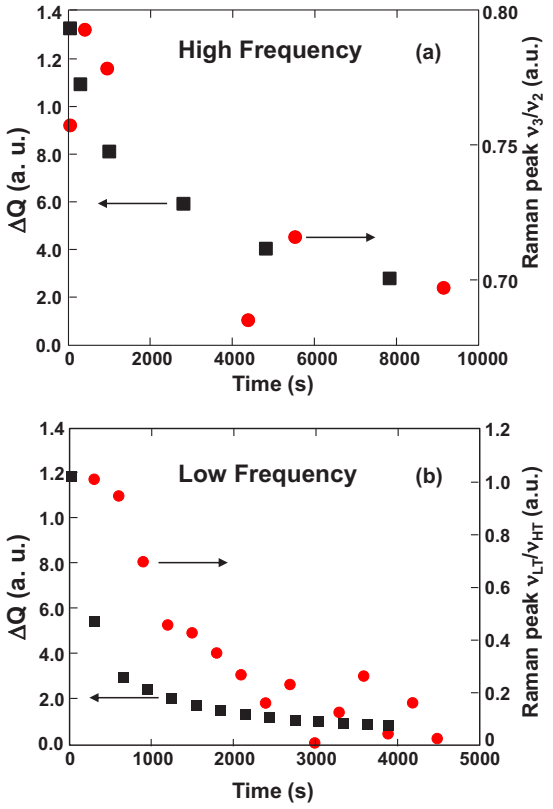

FIG. 8. Decay characteristics of trapped charge, ΔQ, and (a) relative intramolecular Raman peak (ν_3/ν_2) and (b) relative intermolecular Raman peak (ν_{LT}/ν_{HT}) under photoexcitation.

After $t = 4300$ s, the pentacene film was repeatedly illuminated for periods of 150 s with light having photon energies between 1 and 3 eV. Raman spectra were recorded during the 150 s interval between illuminations. The intensity of the LT peak at 50 cm^{-1} decreased, while the intensity of the HT peak at 44 cm^{-1} increased, indicating recovery of the initial HT phase after illumination for about 4000 s. Since electron traps in pentacene are distributed between energy levels of 1.8 and 2.5 eV in the gap states [32,33], illumination with a photon energy of 1–3 eV should release the electrons trapped at the interface (Fig. 5) and the released electrons should play a role in the transformation from the LT phase into the HT phase (Fig. 6). These results clearly indicate that electrons are trapped in pentacene under positive gate BS and they stabilize the LT phase, which is usually unstable in ZCPEN films on a dielectric surface, as was previously pointed out [11].

Corresponding changes in the intramolecular Raman spectra in the HF region and the relative peak intensity ν_3/ν_2 are shown in Figs. 7(a) and 7(b). Since the 1156 cm^{-1} peak, ν_1, was not clearly resolved, all the spectra were normalized at the intensity of the 1158 cm^{-1} peak, ν_2. Figure 7(a) shows five intramolecular Raman spectra measured after the BS (AS), in the dark (DK), and during photoexcitation (PE); the indicated times are from the point at which the BS was removed. The times measured from after the photoexcitation started (+0.3, +1.8, and + 3.3 h) are also indicated in brackets for the three spectra measured during PE. After removing the BS and photoexcitation, the relative peak intensity at 1163 cm^{-1} (ν_3/ν_2) drastically decreased, as was also in the case for ν_{LT}/ν_{HT} in Fig. 7(b). By comparing the transient decay of the two relative Raman peak intensities, ν_3/ν_2 and ν_{LT}/ν_{HT}, and the amount of trapped charge, ΔQ, as a function of time after the photoexcitation [Figs. 8(a) and 8(b)], we can estimate the difference in the spatiotemporal dynamics during the phase transformation. In the high-frequency region, ν_3/ν_2 decreases immediately upon release of ΔQ by the photoexcitation, while in the low-frequency region ν_{LT}/ν_{HT} decreases relatively slowly, with approximately a 2000 s delay compared with the ΔQ decay. The difference in the decay characteristics of the relative Raman peak intensities for intra- and intermolecular vibrations reflects the different microscopic mechanisms. In case of the intramolecular peak, the C-H in-plane vibration of the atoms at the ends of the pentacene molecules can be activated once the charge detrapping releases the individual molecular motion. On the other hand, the phonon lattice mode needs some volume of the corresponding polymorph region to grow, which takes time after the photoexcitation releases the trapped charge, as the MD simulation described below shows [23].

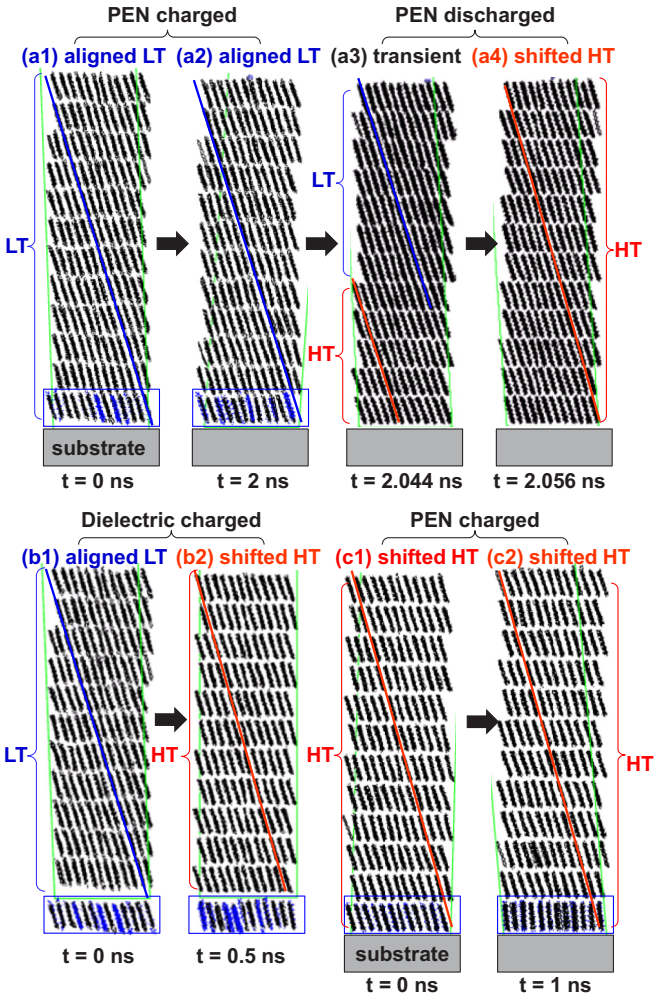

FIG. 9. Multilayer MD simulation for effect of trapped electrons and the trapped positions on the stability of polymorphous microstructures of pentacene films placed on dielectric substrate; (a1), (a2) electrons trapped in first pentacene LT layer, (a3), (a4) electrons removed from first pentacene LT layer, (b1), (b2) electrons trapped at dielectric substrate with LT layer, and (c1), (c2) electrons trapped in first pentacene HT layer.

C. Multilayer MD simulation

To reveal the microscopic origin of the relationship between the polymorph, vibration, and charge trapping, we conducted a multilayer MD simulation to investigate the effect of charge trapping on the stability of the microstructures and intensities of molecular vibration in different microstructural environments. Figure 9 shows the effect of electron trapping and the positions at which they become trapped on the stability of LT- and HT-phase pentacene films on a dielectric substrate. The pentacene films consisted of 12 monolayers with the first pentacene monolayer adjacent to the dielectric substrate charged with electrons [(a1) and (a2)] or with the dielectric substrate charged with electrons [(b1) and (b2)]. In cases (a1) and (a2), a total of 25% of the pentacene molecules in the first layer is randomly selected and each of the selected molecules is charged with an elementary charge. The charge distribution on the dielectric surface for case (b1) is built up from the charged first monolayer of pentacene by burying the same charges in the dielectric surface. Snapshots of the structures with the charged first layer of pentacene at $t = 0$ (a1), just before discharge at $t = 2$ ns (a2), and just after discharge at $t = 2.044$ ns (a3) and $t = 2.056$ ns (a4) are shown from left to right in the upper panel. All structures are viewed along the a axis. The LT phase is stabilized by electrons trapped in the first pentacene layer [(a1) and (a2)], and the discharge applied at $t = 2$ ns clearly removes the stabilizing effect [(a3) and (a4)]. The LT phase transforms into the HT phase, which appears at the bottom of the substrate surface with a time constant of 56 ps, as shown in our previous MD simulation [23]. In the case of the charged dielectric surface [(b1) and (b2)], the LT phase is not stabilized, and it immediately transforms into the HT phase, as in the case without charges. These results indicate that the electrons have to be trapped in the pentacene molecules at the interface and not on the dielectric surface in order to stabilize the LT phase during the gate BS; this was previously clarified in Ref. [11].

Overlapping the images of many pentacene wire-frame models gives a means of visualizing the amount of fluctuation in each polymorph. In the charged LT phase [(a1) and (a2)], the pentacene images make interlayer connections and the layers undulate, meaning there is a large longitudinal fluctuation even on the flat dielectric surface. In contrast, in the HT phase after discharge [(a3) and (a4)], the images show a clear interlayer spacing and substantially flat layers. A large static displacement collectively occurs among collinearly aligned pentacene molecules in the LT phase [the blue lines in (a1) and (a2)] since a displaced molecule in the first monolayer pushes all the aligned adjacent molecules. This collective displacement should stabilize or pin the LT phase even on a dielectric surface, as the displaced molecules penetrate the adjacent layers and these "anchor" molecules prevent a transformation into the HT phase in which molecules in adjacent layers would be shifted [the red lines in (a4) and (b2)]. As the molecular fluctuation is suppressed by the interaction with the flat dielectric substrate [(a3), (a4), and (b2)], the static molecular disorder along the long axis is considered to be induced by Coulomb repulsion between localized electrons in the first monolayer [(a1) and (a2)]. The large disorder or displacement of the charged LT molecular configuration depends on a subtle balance between the van der Waals force between molecules, their interaction with the substrate, and the Coulomb force between localized charges at the interface and is modulated by thermal molecular fluctuations. Therefore, once the disorder becomes unstable due to thermal fluctuations, the charge localization should become transient [4,5]. Additionally, for comparison, we simulated the stability of the charged HT phase [(c1) and (c2)], for which the time evolution of the HT phase with a charged first monolayer was monitored. We could not observe the transition from the charged HT phase to the LT phase (see Fig. 4).

Our multilayer MD simulation quantitatively revealed that in the charged LT phase, the disorder induced by trapped charge becomes static. Here, Fig. 10 indicates the pentacene molecular vibration power spectrum for (a) "bulk" LT and HT phases without charge and for (b) "thin films" of the charged LT phase and discharged HT phase. Abrupt increases at lower frequency in both the LT bulk and LT film are artefacts due

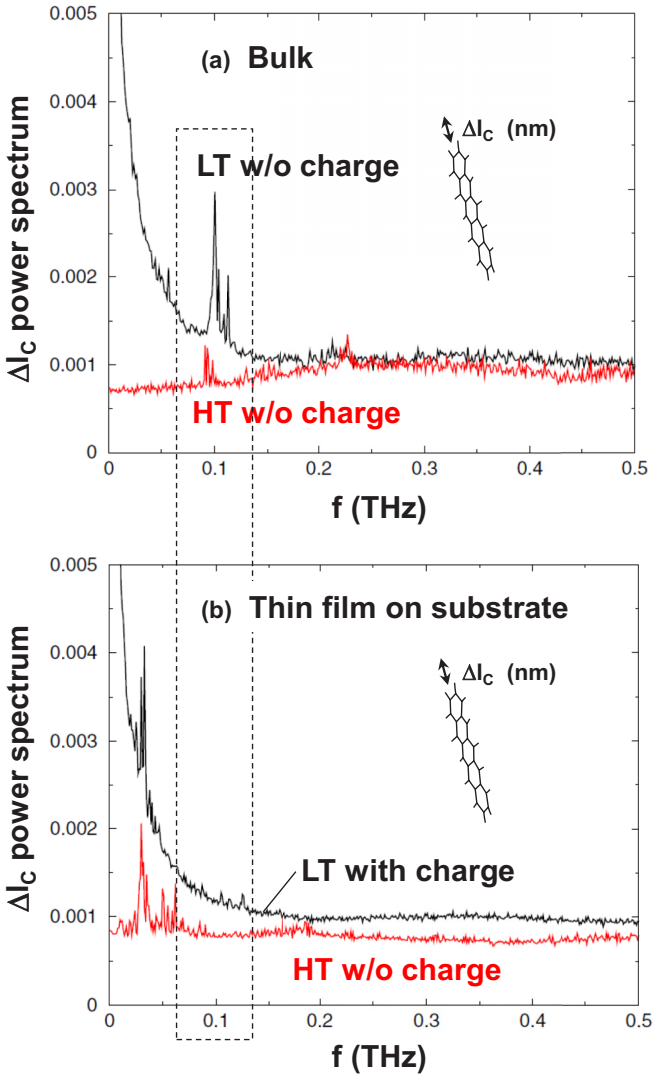

FIG. 10. MD-simulated molecular vibrational power spectra of (a) bulk LT and HT phases and (b) charged LT phase and discharged HT phase in thin-film form.

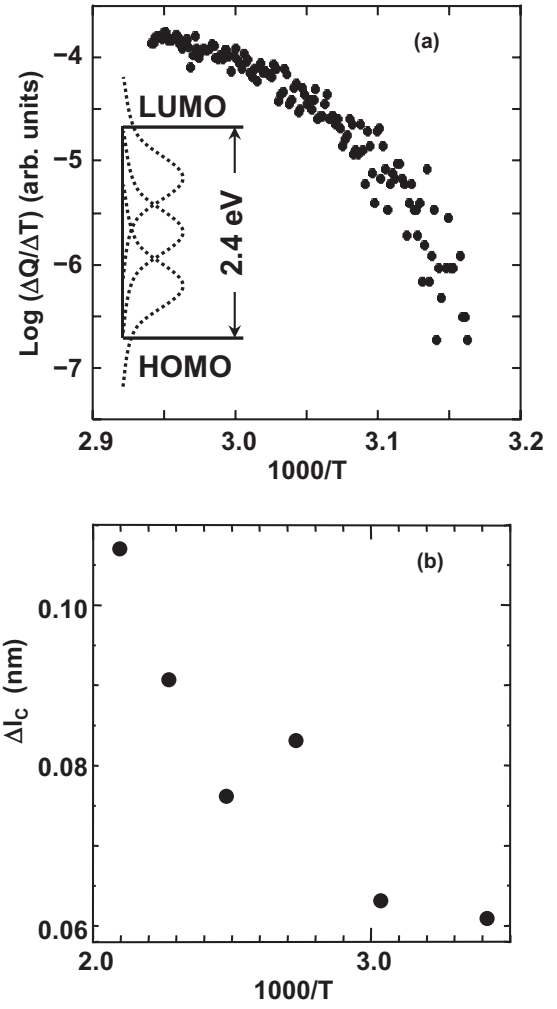

FIG. 11. (a) Nonlinear Arrhenius plot of thermally detrapped charge, ΔQ; (b) MD-simulated thermal fluctuation of molecular motion along long axis, Δl_c, in the LT phase of pentacene molecules.

to the instability of the unit cell for MD simulation. In bulk PEN, a strong vibrational peak appears around 0.1 THz and the peak in the LT phase is more than five times larger than it is in the HT phase. This increase should be due to the interlayer molecular alignment in LT-phase PEN molecules making this large fluctuation possible and making the bulk LT-phase stable [23]. In thin films, on the contrary, there are no such peaks in this frequency region for either the charged LT phase or the discharged HT phase. These results suggest that the charged LT-phase in thin films is stable because the molecular vibrations in the thin films are much smaller than in bulk samples and this makes the charge localization permanent with reduced and fixed transfer integrals. We could not obtain the power spectrum for the discharged LT phase because it is very unstable on a flat substrate and transforms immediately into the HT phase [(a3) and (a4) in Fig. 9].

The above results suggest that molecular vibration is crucial for delocalization of self-trapped electrons from the frozen disorder in the LT phase [4,5]. To experimentally confirm the effect of molecular vibration on delocalization of self-trapped electrons from static disorder in the LT phase, the thermally stimulated current was measured. Thermally stimulated currents obtained from the linear slope of the Arrhenius plot give an estimate of the trap depth [34]. However, as shown in Fig. 11(a), the Arrhenius plot for self-trapped electrons in the frozen disorder in the LT phase is nonlinear (this nonlinearity has been reported in the literature [35,36]), indicating that the depth of the trap states is temperature dependent. After the gate-BS, the drain current (with $Vg = Vd = -5V$) was monitored while elevating the temperature, T, at a constant rate of 1 °C/min from room temperature up to 130 °C. The trapped electrons, ΔQ, were released as T increased. The activation energy of the electron trapping states obtained from the slope of the Arrhenius plot decreases with temperature from 2.17 to 0.31 eV. Its average value is 0.94 eV below the lowest unoccupied molecular orbital (LUMO) level, which is close to the values measured by different methods [32,33]. The MD-simulated molecular displacement, Δl_c, increases with temperature [Fig. 11(b)], indicating that the disorder becomes dynamic and the probability of trapped charge delocalization

should increase with temperature, as theoretically predicted [4]. This experimentally observed decrease in depth of the electron trapping state with temperature is likely due to thermal energy melting the frozen static disorder of the charge-trapping LT phase and enabling the self-trapped electrons to escape quantum mechanically via transfer integral fluctuation as well as classically via hopping.

D. Dynamic disorder and mobility

The mobility increase upon thermal annealing and accompanying an irreversible transformation from the LT to the HT phase should be caused by the decrease in fluctuation of the transfer integral [4–7]. Here, the statistical distributions of the transfer integral for the LT phase and the HT phase were calculated using molecular configurations determined from multilayer MD simulations. The results shown in Fig. 12(a) are the positions of the atoms (black dots) and the center of gravity (red dots) of the first monolayer pentacene molecules on the dielectric substrate for the charged LT phase (upper) and the discharged HT phase (lower). Those in Fig. 12(b) are the three directions $A(A')$, B, and C for the transfer integrals in a $3 \times 2 \times 1$ pentacene supercell, while those in Fig. 12(c) are the statistical distributions of the three different nearest-neighbor transfer integrals for the two phases. The transfer integral values were calculated over 72 pairs in 84 molecules in the first monolayer. For the charged LT phase, the averaged transfer integral J and standard deviation ΔJ due to static disorder for pairs of molecules were respectively 140 and 397 cm^{-1}, whereas those for the HT phase without charge were 230 and 235 cm^{-1}. The fluctuation in the transfer integral, defined as $\Delta J/J$, for the charged LT phase (2.70) is more than twice as large as that for the discharged HT phase (1.02). As shown in Fig. 12(a), these results indicate that the maximum fluctuation of molecular out-of-plane dynamic disorder (4.0 A) for the charged LT phase is more than three times larger than that for the discharged HT phase (1.3 A). This is consistent with the experimentally observed mobility, respectively, 0.48 and 0.7 cm^2/Vs before and after annealing, since the mobility decreases with increased transfer-integral fluctuation, $\Delta J/J$ [4,5].

Figure 13 summarizes the relationship between mobility, transfer integral disorder $\Delta J/J$, and the intramolecular Raman peak as a function of molecular displacement disorder, Δl_c. Here, the mobility and $\Delta J/J$ data for the TF phase are taken from the Supplemental Material of Ref. [5], and references therein. The MD simulation indicated the maximum vertical molecular displacements, Δl_c, of 0.4, 0.25, and 0.13 nm for the charged-LT, discharged-LT, and HT polymorphs, respectively. The value for the discharged-LT phase was one calculated for the bulk LT phase [23] because the LT phase is unstable in thin-film form. As Δl_c has no explicit value for the TF phase, we tentatively assumed it to be zero, since the transfer integral fluctuation is much smaller than those of other polymorphs. It is reasonable that the mobility decreases with increasing molecular displacement, Δl_c, because it has been observed experimentally [7], and further, it has been theoretically proposed to accompany increased transfer integral disorder, $\Delta J/J$ [5]. Although the mobility for the TF phase is taken from Ref. [5] and the relatively large

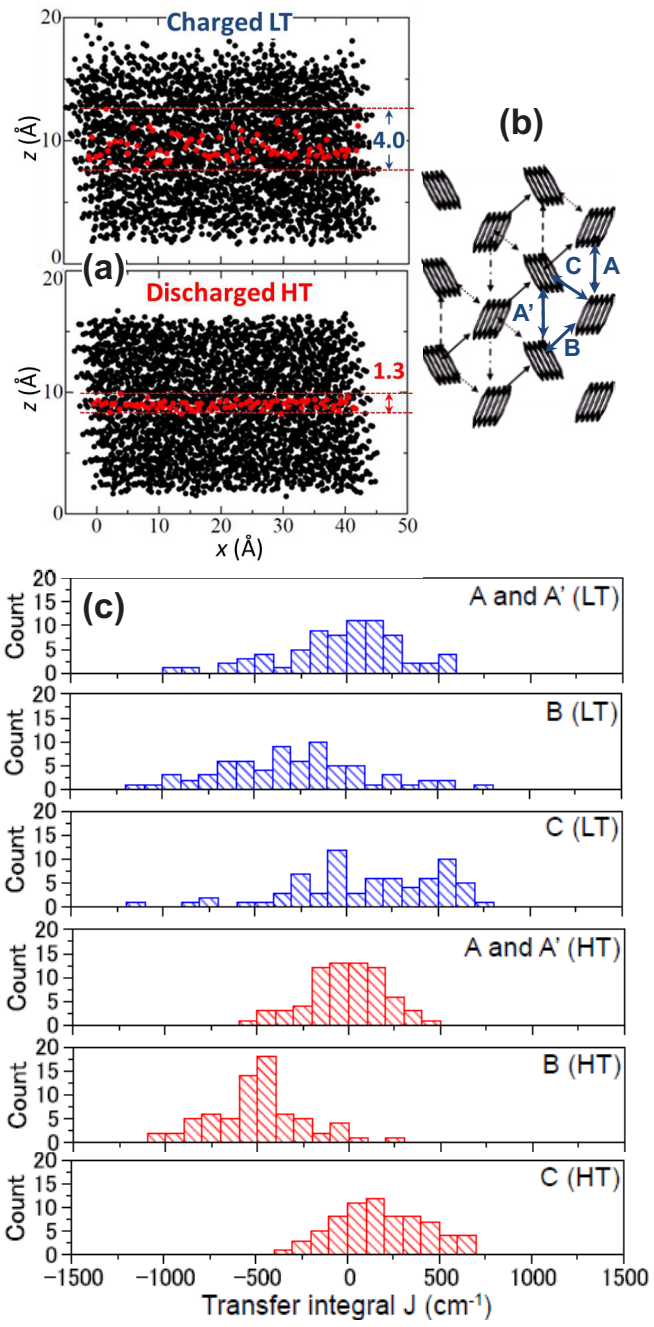

FIG. 12. (a) Positions of atoms (black dots) and center of gravity (red dots) of the first-monolayer pentacene molecules on dielectric substrate for the charged LT phase (upper) and the discharged HT phase (lower); (b) Three directions $A(A')$, B, and C for transfer integrals in $3 \times 2 \times 1$ pentacene supercell; (c) Statistical distributions of the three different nearest-neighbor transfer integrals for the two phases.

fluctuation (1.45 ± 0.85 cm^2/Vs, not shown in Fig. 13) is probably due to the different device configurations and measurement conditions, the result that the mobility of the HT phase is lower than that of the TF phase is supported by the report [37] in which x-ray diffraction revealed that the mobility of the TF phase was drastically reduced by solvent vapor annealing inducing a phase transformation to the HT

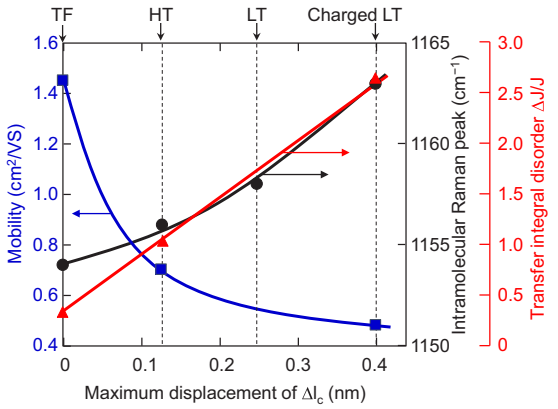

FIG. 13. Relationship between mobility, transfer integral disorder $\Delta J/J$, and intramolecular Raman peak as a function of maximum molecular displacement disorder, Δl_c.

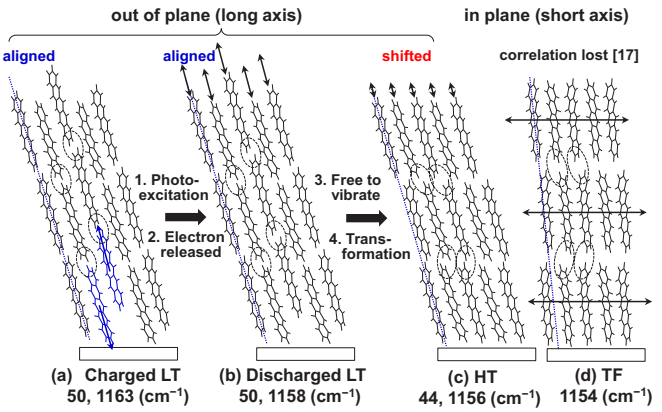

FIG. 14. Cross-sectional pentacene molecule arrangements on dielectric surface for (a) charge-trapped LT phase (corresponding inter- and intramolecular Raman peaks at 50 and 1163 cm^{-1}), (b) discharged LT phase just after photoexcitation (50 and 1158 cm^{-1}), (c) discharged HT phase (44 and 1156 cm^{-1}), and (d) TF phase (1154 cm^{-1}). The meanings of the blue dashed lines, ovals, and black double-headed arrows are explained in the text.

phase. The increase in Δl_c should strengthen the interaction between molecules in adjacent layers, and the interaction especially affects the C-H in-plane vibration of atoms at the ends of the pentacene molecules, resulting in changes in the intramolecular Raman peaks at 1154 cm^{-1} (TF), 1156 cm^{-1} (HT), 1158 cm^{-1} (LT), and 1163 cm^{-1} (charged LT).

The above results clarify the importance of the polymorphs in the pentacene thin films to the description of the microscopic transient localization scenario with their out-of-plane dynamic disorder [4,5]. In this scenario, high-mobility molecular crystals can be identified by considering only the sign and relative magnitude of the electronic coupling, or the transfer integral $\Delta J/J$, between nearest-neighbor molecules. The reason the hole mobility of pentacene is relatively low is that the opposite sign of the coupling of a pentacene molecule to one of its neighbors limits the localization length, a crucial parameter determining the charge carrier mobility. However, those who proposed this scenario did not investigate the effects of polymorphs on the charge carrier mobility of pentacene, because they ignored such polymorphic disorders [4] by using a relatively simple two-dimensional (2D) MD simulation model which may only apply to the TF phase. Here, we successfully simulated the two polymorphous 3D structures of the HT and TF phases and used the vertical displacement of the pentacene molecules (Fig. 12) to investigate the relationship between dynamical disorder, transfer integral fluctuation, and mobility quantitatively (Fig. 13).

E. A unified picture of disorder and localization

Here, we propose a unified picture of the structure-property relationship in pentacene polymorphs that arises from the conflict between in-plane and out-of-plane dynamic and static disorders induced by competition between the van der Waals force, thermal vibration, and electronic Coulomb repulsive forces. Figure 14 depicts cross-sectional pentacene molecule arrangements on a dielectric surface. Figure 14(a) shows the charge-trapped LT phase (corresponding to the intramolecular Raman peak at 1163 cm^{-1}), Fig. 14(b) shows the discharged LT phase just after photoexcitation (1158 cm^{-1}), Fig. 14(c) shows the HT phase (1156 cm^{-1}), and Fig. 14(d) shows the TF phase (1154 cm^{-1}). The blue dashed lines are guides for the eye that indicate the alignment of molecules in adjacent layers. Ovals indicate interactions between C-H atoms at the ends of pentacene molecules in adjacent layers, which determines the intramolecular Raman peak values. Black double-headed arrows indicate amounts and directions of molecular motion for each polymorph. The dominant molecular motion in the LT and HT phases is out of plane along the long axis, whereas that in the TF phase, it is in-plane along the short axis because of the stronger van der Waals force between adjacent molecules that are standing at a steeper inclination (84–86° for the TF phase and 69° for the HT and LT phases) [26]. The experimental evidence will be discussed later, but here, we stress that our previously proposed charge trapping (permanent localization) mechanism with static disorder [11] is seamlessly situated in this picture. As shown in Figs. 2 and 4, BS in ZCPEN films with electrons that have accumulated at the interface with the gate dielectric induces a microstructure transformation from the HT phase to the LT phase by inducing electron trapping (localization), as shown in Fig. 14(a). In contrast to the HT phase with a shifted molecular alignment in adjacent layers, the LT phase with the aligned molecular configuration can induce dynamic disorder one order of magnitude larger than that induced by the HT phase, as estimated from our MD simulation [23]. In the charge-trapped LT phase, the molecular dynamic disorder is frozen (Fig. 10). We conjecture that the static disorder in the LT phase is a result of the repulsive Coulomb force of trapped electrons causing neighboring charged pentacene molecules to move in opposite directions [blue-colored pentacene molecules with blue arrows in Fig. 14(a)]. Once the localized electrons are released by photoexcitation, molecules become free to vibrate immediately [black double-headed arrows in Fig. 14(b)], as shown in the transient properties of the intramolecular Raman peaks in Fig. 8(a). The molecular vibration triggers a gradual microstructure transformation from the charge-trapped LT phase to the discharged HT phase,

as shown experimentally in the transient properties of the intermolecular Raman peaks of Fig. 8(b) and theoretically in the multilayer MD simulation of Fig. 9 (a3) and (a4), although the transition time of the simulation is much shorter than that of the experiment probably because of the smaller cell volume of the simulation. We conclude that a certain amount of localized charges enhances the disorder and makes it static, resulting in the self-trapping (self-localization) scenario [11]. We expect that the depth of the trap states from the LUMO (conduction band edge) level increases with the amount of static disorder. The fluctuation in Δl_c increases with increasing temperature, as shown in Fig. 11(b), and this results in detrapping of the localized electrons in the pentacene molecules quantum mechanically via the fluctuating transfer integral and classically via hopping. This synergetic effect should be the origin of the nonlinear Arrhenius behavior of the thermally stimulated current shown in Fig. 11(a), indicating a reduced trap depth with temperature.

Next, to explain how the transport properties differ depending on the polymorphous structures, we will start with the thin-film phase that shows the highest mobility and the lowest dynamic disorder, as shown in Fig. 13. Low-frequency Raman peak modes involving interlayer interactions are never observable in the typical TF structures, and it is reported that the TF phase is intrinsically a 2D structure, in which dynamical correlations between adjacent layers are weak or nonexistent, as schematically shown in Fig. 14(d) [17]. This should be due to the out-of-plane dynamic disorder being suppressed by the relatively higher van der Waals force constant between intralayer molecules vertically standing on the substrate surface, and this results in the main molecular motion being in-plane along the short axis. However, in the HT phase with intralayer molecules inclined with a relatively lower van der Waals force and a shifted order between adjacent layers, small out-of-plane molecular motions are allowed; this increases the transfer integral fluctuation, $\Delta J/J$, causing a mobility decrease. Furthermore, in the LT phase with aligned molecules in adjacent layers, the out-of-plane molecular motions are further enhanced to increase $\Delta J/J$ and decrease the mobility through the increased dynamic disorder. Thus, the transient localization scenario for charge transport and the static localization scenario for charge trapping can be described in a unified picture taking into account both dynamic and static disorder. Recently, semiconductor molecules with high mobility and stability have been designed by taking care of their polymorphs and suppressing and/or eliminating their sensitivity to the out-of-plane disorder [38,39]. We hope this unified picture of the benchmark semiconductor molecule pentacene will be helpful for understanding the disorder-localization relationships in these new materials.

Finally, we would like to stress that our model of the multilayer MD simulation is crucial to reproducing the experimentally observed stabilities of the HT and LT phases both in bulk and TF forms at room temperature and normal pressure. It is a flexible (all-atom) model of pentacene, unlike the rigid sort of molecular model that is frequently used to study molecular crystalline systems. Here, we compared three flexible pentacene models with one using the Lennard-Jones (12-6)-type potential and two other models using the Buckingham-type (exp-6) potential for the intermolecular interactions [23]. The Buckingham-type intermolecular interaction potential is also frequently used to study molecular crystalline systems. Among these three models, we found that only the first one reproduced the experimentally observed polymorphous stabilities [23]. This implies that a flexible molecular model with a proper intermolecular interaction is crucial to describing the polymorphs of pentacene and probably other molecular crystalline systems. Recently, it has been pointed out that insight into the relation between the impact of low frequency vibrations on charge transport and the molecular semiconductor structure can be gained from combined theoretical and experimental studies of polymorphs [8]. Our combined studies of pentacene polymorphs should therefore contribute to the creation of efficient guidelines for the rational design of high-mobility molecular semiconductors.

IV. CONCLUSIONS

In order to reveal the effects of polymorphs on the microscopic relationship between structural disorder and charge localization dynamics in a van-der-Waals-bonded molecular semiconductor, field-effect transistors with ZCPEN films were prepared as a model system having a pseudocrystalline molecular microstructure clearly showing specific polymorphic phases, and their molecular vibrations were monitored by using *in situ* micro-Raman spectroscopy to measure both the intermolecular and the intramolecular vibrational peaks. Transformations from the HT phase with reduced molecular vibration along the long axis that were induced by electron localization in pentacene molecules at the channel interface region and transformations from the LT-phase with increased molecular vibration that were induced by electron delocalization from pentacene molecules were clearly observed under gate-BS, photoexcitation, and thermal annealing. Multilayer MD simulations revealed that electrons are localized in each pentacene molecule and stabilize the charge-localized LT phase by freezing the vertical molecular disorder; this picture is consistent with experimentally observed nonlinear Arrhenius plots indicating that the depth of electron trap states is decreased by thermally enhanced out-of-plane molecular vibration. Furthermore, it was shown that the intramolecular Raman peak, originating from the C-H in-plane vibration of atoms at the ends of the pentacene molecules, is in good correlation with the amount of out-of-plane molecular displacement most influential to the charge localization and the mobility reduction due to transfer integral fluctuation, the amount of which differed largely between polymorphs.

On the basis of these results, we proposed a unified picture to describe the relationship between structural disorder and localization dynamics in pentacene polymorphs that is induced by competition between van der Waals force, thermal vibration, and electronic Coulomb repulsive force under interaction with the substrate surface. This picture treats the transient and permanent localizations on the same footing by taking account of the out-of-plane dynamic and static disorder, and it clarifies how the transient localization due to dynamical molecular motions originates from *Anderson localization* [19].

ACKNOWLEDGMENTS

M.A. and M.K. thank Professor R. Friend of the Cavendish Laboratory and Dr. D. Williams of Hitachi Cambridge Laboratory for their continuous support. They also thank the EPSRC/Cambridge Integrated Knowledge Centre for financial support (ROOT project). M.A. thanks Dr. J. Winfield of the Cavendish Laboratory for measuring intramolecular Raman peaks. T.B.K. and C.M.D. thank Hitachi for funding. M.A., T.B.K., and M.Y. thank Professor A. Girlando of Parma University for his fruitful discussions.

[1] O. Ostroverkhova, Chem. Rev. **116**, 13279 (2016).
[2] H. Sirringhaus, Adv. Mater. **26**, 1319 (2014).
[3] A. Y. B. Meneau, Y. Olivier, T. Backlund, M. James, D. W. Breiby, J. W. Andreasen, and H. Sirringhaus, Adv. Funct. Mater. **26**, 2326 (2016).
[4] S. Fratini, D. Mayou, and S. Ciuchi, Adv. Funct. Mater. **26**, 2292 (2016).
[5] S. Fratini, S. Ciuchi, D. Mayou, G. Trambly de Laissardière, and A. Troisi, Nat. Mater. **16**, 998 (2017).
[6] A. S. Eggeman, S. Illig, A. Troisi, H. Sirringhaus, and P. A. Midgley, Nat. Mater. **12**, 1045 (2013).
[7] S. Illig, A. S. Eggeman, A. Troisi, L. Jiang, C. Warwick, M. Nikolka, G. Schweicher, S. G. Yeates, Y. H. Geerts, J. E. Anthony, and H. Sirringhaus, Nat. Commun. **7**, 10736 (2016).
[8] A. Y. Sosorev, D. R. Maslennikov, O. G. Kharlanov, I. Y. Chernyshov, V. V. Bruevich, and D. Y. Paraschuk, Phys. Status Solidi RRL 1800485 (2018).
[9] O. D. Jurchescu, D. A. Mourey, S. Subramanian, S. R. Parkin, B. M. Vogel, J. E. Anthony, T. N. Jackson, and D. J. Gundlach, Phys. Rev. B **80**, 085201 (2009).
[10] A. O. F. Jones, B. Chattopadhyay, Y. H. Geerts, and R. Resel, Adv. Funct. Mater. **26**, 2233 (2016).
[11] M. Ando, T. B. Kehoe, M. Yoneya, H. Ishii, M. Kawasaki, C. M. Duffy, T. Minakata, R. T. Phillips, and H. Sirringhaus, Adv. Mater. **27**, 122 (2015).
[12] A. Brillante, I. Bilotti, R. G. Della Valle, E. Venutia and A. Girlando, Cryst. Eng. Comm. **10**, 937 (2008) and references therein.
[13] T. Jentzsch, H. J. Juepner, K.-W. Brzezinka, and A. Lau, Thin Solid Films **315**, 273 (1998).
[14] H.-L. Cheng, W. Y. Chou, C. W. Kuo, F. C. Tang, and Y. W. Wang, Appl. Phys. Lett. **88**, 161918 (2006).
[15] H.-L. Cheng, W. Y. Chou, C. W. Kuo, Y. W. Wang, Y.-S. Mai, F. C. Tang, and S.-W. Chu, Adv. Funct. Mater. **18**, 285 (2008).
[16] A. Brillante, R.G. Della Valle, L. Farina, A. Girlando, M. Masino, and E. Venuti, Chem. Phys. Lett. **357**, 32 (2002).
[17] A. Brillante, I. Bilotti, R. G. Della Valle, E. Venuti, A. Girlando, M. Masino, F. Liscio, S. Milita, C. Albonetti, P. D'angelo, A. Shehu, and F. Biscarini, Phys. Rev. B **85**, 195308 (2012).
[18] A. Girlando, M. Masino, A. Brillante, T. Toccoli, and S. Iannotta, Crystals **6**, 41 (2016).
[19] P. W. Anderson, Phys. Rev. **109**, 1492 (1958).
[20] C. M. Duffy, J. W. Andreasen, D. W. Breiby, M. M. Nielsen, M. Ando, T. Minakata, and H. Sirringhaus, Chem. Mater. **20**, 7252 (2008).
[21] W. Pisula, A. Menon, M. Stepputat, I. Lieberwirth, U. Kolb, A. Trancz, H. Sirringhaus, T. Pakula, and K. Muellen, Adv. Mater. **17**, 684 (2005).
[22] T. Siegrist, C. Besnard, S. Haas, M. Schiltz, P. Pattison, D. Chernyshov, B. Batlogg, and C. Kloc, Adv. Mater. **19**, 2079 (2007).
[23] M. Yoneya, M. Kawasaki, and M. Ando, J. Mater. Chem. **20**, 10397 (2010).
[24] J. M. Winfield, C. L. Donley, R. H. Friend, and J.-S. Kim, J. Appl. Phys. **107**, 024902 (2010).
[25] See Supplemental Material at http://link.aps.org/supplemental/10.1103/PhysRevMaterials.3.025601 for our multilayer MD simulation.
[26] M. Yoneya, M. Kawasaki, and M. Ando, J. Phys. Chem. C **116**, 791 (2012).
[27] E. F. Valeev, V. Coropceanu, D. A. da Silva Filho, S. Salman, and J.-L. Brédas, J. Am. Chem. Soc. **128**, 9882 (2006).
[28] H. Ishii, K. Honma, N. Kobayashi, and K. Hirose, Phys. Rev. B **85**, 245206 (2012).
[29] H. Ishii, N. Kobayashi, and K. Hirose, Phys. Rev. B **95**, 035433 (2017).
[30] A. Brillante, I. Bilotti, R. G. Della Valle, E. Venuti, M. Masino, and A. Girlando, Adv. Mater. **17**, 2549 (2005).
[31] T. Hallam, C. M. Duffy, T. Minakata, M. Ando, and H. Sirringhaus, Nanotechnology **20**, 025203 (2009).
[32] K. Harada, M. Riede, K. Leo, O. R. Hild, and C. M. Elliott, Phys. Rev. B **77**, 195212 (2008).
[33] Y. S. Yang, S. H. Kim, J.-I. Lee, H. Y. Chu, L.-M. Do, H. Lee, J. Oh, T. Zyung, M. K. Ryu, and M. S. Jang, Appl. Phys. Lett. **80**, 1595 (2002).
[34] T. Sakurai, Phys. Rev. B **40**, 11817 (1989).
[35] V. Aquilanti, K. C. Mundim, M. Elango, S. Kleijn, and T. Kasai, Chem. Phys. Lett. **498**, 209 (2010).
[36] A. C. P. Rosa Jr., P. Vaveliuk, K. C. Mundimd, and M. A. Moreta, Physica A **450**, 317 (2016).
[37] D. J. Gundlach, T. N. Jackson, D. G. Schlom, and S. F. Nelson, Appl. Phys. Lett. **74**, 3302 (1999).
[38] H. Chung and Y. Diao, J. Mater. Chem. C **4**, 3915 (2016).
[39] A. Yamamoto, Y. Murata, C. Mitsui, H. Ishii, M. Yamagishi, M. Yano, H. Sato, A. Yamano, J. Takeya, and T. Okamoto, Adv. Sci. **5**, 1700317 (2018).